JACS
JOURNAL OF THE AMERICAN CHEMICAL SOCIETY
pubs.acs.org/JACS
Article

Multidentate Coordination Chemistry Enables Adaptive Ionic Cross-Linking of Conductive Binder for Reversible Silicon Anodes

Lu Wang,[‖] Hao Zhang,[‖] Zhibo Song,[‖] Haoliang Wang, Yumeng Lan, Zu-Wei Yin, Luyi Yang,* and Feng Pan*

Cite This: *J. Am. Chem. Soc.* 2026, 148, 7919–7930

Read Online

ACCESS | Metrics & More | Article Recommendations | Supporting Information

ABSTRACT: Conductive binders present a potential solution to the volumetric instability of silicon anodes; yet their low molecular weight and limited mechanical robustness demand reversible interactions to establish stable, adaptive cross-linked networks. Building on this concept, coordination bonds with their reversible dynamics serve as a key strategy for constructing such adaptive polymer networks, though their structure–property relationships remain elusive. This work seeks to unveil the key mechanism by which ionic coordination structures govern the performance of conductive binders in silicon anodes and to establish a universal, coordination-based design strategy for ion-cross-linked binders. It is revealed that the multidentate bridge coordination between carboxylate groups and Fe^{3+} simultaneously reinforces mechanical strength and maintains uniform polymer–silicon interactions, achieving the balance essential for stable cycling. Benefiting from such coordination structure, the Fe^{3+}-coordinated conductive binder well accommodates silicon's volume fluctuations, enabling reversible electrode deformation. The enhanced structural adaptability also spatially confines the growth of the solid-electrolyte interphase, preventing its thickening and the dilution of the LiF-rich phase by undesirable species. As a result, the rational binder design translates into a significant boost in the electrochemical performance of the silicon electrodes. Rooted in coordination chemistry, this work offers theoretical insights into the design of adaptive networks for high-volume-changing battery materials.

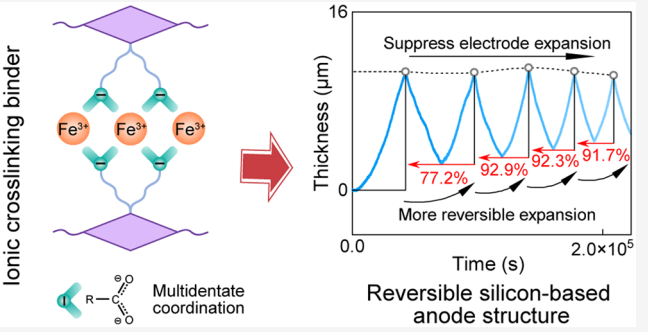

1. INTRODUCTION

In recent years, silicon (Si)-based anodes have emerged as a leading candidate among high-performance anode materials owing to their exceptionally high theoretical specific capacity, low operating potential, abundant reserves, and environmental friendliness. However, the vast volumetric changes (up to 300%) during the lithiation/delithiation process lead to particle pulverization, delamination, and uncontrolled thickening of the solid-electrolyte interphase (SEI), severely hindering the widespread commercialization of Si-based anodes.[1−4] In order to address these challenges, researchers have conducted extensive studies focusing on material structure optimization, binder design, and electrolyte regulation.

Our previous studies revealed that the disruption of the conductive network caused by irreversible volume expansion is one of the key factors contributing to the performance degradation of Si-based anodes.[5,6] Therefore, designing conductive binders with both robust mechanical strength and strong adhesion offers a multifaceted strategy to mitigate this issue.[7−14] However, their rigid conjugated backbones result in low molecular weights and limited mechanical robustness, making them ill-suited for accommodating the volumetric fluctuations of Si anodes. Constructing a cross-linked binding network through enhanced intermolecular interactions offers an effective strategy to mitigate the structural degradation. Despite its potential benefits, cross-linking the binder often compromises its dispersibility in the slurry, leading to detrimental uneven stress distribution within the electrode. To address this issue, we developed an in situ photo-cross-linking strategy based on thiol–ene click chemistry, which forms a resilient conducting network while effectively preventing particle agglomeration.[15]

Compared to covalent cross-linking, ionic cross-linking using metal ions offers advantages in ease of operation and reversibility: it not only avoids the challenge of controlling the degree of cross-linking, but also endows the resulting network with self-healing capability. The ion-cross-linking strategy offers a new, practical, and effective solution to overcoming the mechanical limitations of conductive binders,

Received: December 19, 2025
Revised: January 30, 2026
Accepted: February 3, 2026
Published: February 10, 2026

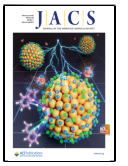

https://doi.org/10.1021/jacs.5c22740
J. Am. Chem. Soc. 2026, 148, 7919–7930

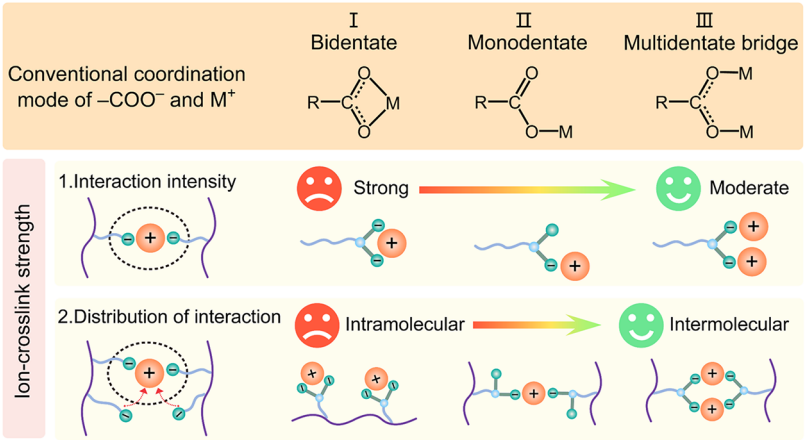

Figure 1. Schematic illustration of the typical coordination between carboxylate anions and metal cations affecting the cross-link strength between polymer chains.

providing important insights into their further development. Given that the coordination structure of ionic binding determines the network structure and properties, a thorough investigation of the coordination mechanisms is of great importance. In previous studies, simple screening criteria (e.g., the hardness of metal ions and their ionic potential[16]) have been proposed. However, in addition to the intrinsic properties of metal ions, the type and spatial configuration of the ligand are equally important and should therefore be investigated as an integrated system.

In this work, the influence of different coordination between carboxylate (COO^-) and metal ions on the uniformity and cross-link strength was explored. Through molecular dynamics simulations and experimental results, we identify Fe^{3+} as the preferred cation, favoring the multidentate bridge coordination with carboxylate-rich conductive polyfluorene (PF-COO^- with the well-established synthetic method)[15] binders to construct a robust and reversible binding network. The addition of Fe^{3+} not only enhances the mechanical properties of the binder network but also ensures a more uniform distribution of cross-link sites within the system, thereby achieving better stress dissipation and facilitating higher reversible expansion. The stable electrode structure and conductive network also help prevent the degradation of the SEI during cycling, enabling the silicon electrode to maintain a high discharge capacity and capacity retention after prolonged cycling. By elucidating the intrinsic influence of ionic coordination chemistry on the mechanical strength and uniformity of polymer networks, this work provides theoretical guidance for designing high-stability binders capable of accommodating volumetric expansion. The widespread presence of the selected carboxylate ligands in high-performance silicon-based binders renders this design strategy broadly applicable across diverse binder systems.

2. RESULTS AND DISCUSSION

2.1. Select Metal Ions Suitable for Ionic Cross-Linking in Conductive Binders

Carboxyl functionalities are considered effective adhesion-promoting motifs in high-performance silicon-based binders, owing to their ability to form hydrogen bonds with hydroxyl groups on the surface of silicon particles and generate ester linkages through thermally induced reactions.[15] When metal ions coordinate with carboxyl groups to form carboxylates, the resulting ionic coordination interactions that enhance inter-molecular forces between polymer chains can take the form of monodentate, bidentate, or multidentate bridging coordination (Figure 1).[17] Compared to the moderately strong multidentate bridge coordination, monodentate and bidentate coordination exhibit excessively strong interactions, leading to overcross-linking, reduced solubility, and brittle electrode structures. In bidentate coordination, the metal ion coordinates with both oxygen atoms of the same carboxylate group, favoring intramolecular interactions, resulting in a local stress concentration that hinders stress dissipation. In monodentate coordination, the uneven distances between the metal ion and the two oxygen atoms lead to asymmetric interactions, hence a nonuniform cross-linked network. Conversely, multidentate bridge coordination provides two nearly equivalent binding sites, which facilitate strong intermolecular interactions between polymer chains, enabling the formation of a uniformly cross-linked network. This coordination mode is therefore considered more favorable for the design of robust binder systems for Si-based anodes.

Herein, the ability of various metal ions (Mg^{2+}, Ca^{2+}, Fe^{3+}, In^{3+}, and Zr^{4+}) to form multidentate bridging coordination with the carboxylate side chains of polyfluorene binder (Figures 2a and S1) was evaluated by cross-validation between molecular dynamics (MD) simulations (Figure S2) and experimental results. The radial distribution function (RDF) analysis reveals that Fe^{3+} is located closer to the oxygen atoms of the carboxylate group (Figure 2a), suggesting a higher tendency to form stable coordination bonds. In contrast, Mg^{2+} and Ca^{2+} exhibit greater distances to the oxygen atoms, suggesting less favorable coordination, likely due to differences in their coordination mode with the ligands. Further investigation of the RDFs between the two types of oxygen atoms (C−O/C═O on the carboxylate group) and the metal ions (Figure 2b) revealed deeper insights into the coordination modes. For Mg^{2+}, Ca^{2+}, In^{3+}, and Zr^{4+}, the distance to the C−O oxygen is shorter than to the C═O oxygen, indicating a predominance of monodentate coordination, which leads to uneven coordination interactions within the network. In contrast, Fe^{3+} exhibits similar distances to both oxygen atoms, suggesting the presence of a multidentate bridge coordination that facilitates a more uniform cross-linked polymer network.

Detailed analysis of the MD simulation results (Figure 2c) reveals that the coordination number (CN) of oxygen atoms

https://doi.org/10.1021/jacs.5c22740
J. Am. Chem. Soc. 2026, 148, 7919−7930

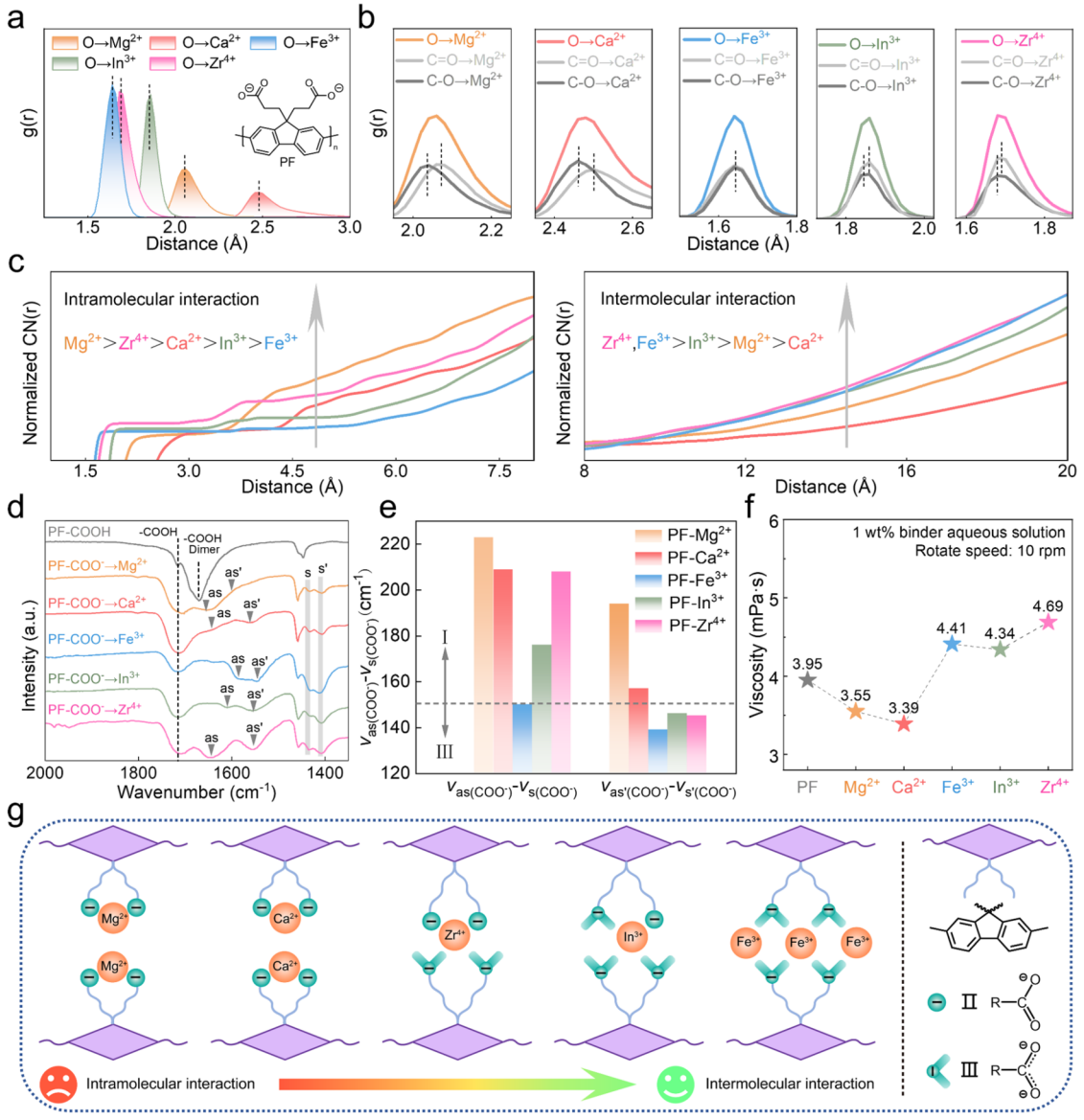

Figure 2. Screen the metal ions that form multidentate bridge coordination with the polyfluorene binder based on molecular dynamics and FTIR spectra. (a) The radial distribution functions (RDF) of metal ions and oxygen atoms belonging to carboxylate groups. (b) The RDF of metal ions and C═O/C−O (two oxygen atoms of the same carboxylate group). (c) The coordination number (CN) of metal ions and oxygen atoms belonging to carboxylate groups. (d) FTIR spectra of conductive binders with different ions added. (e) The wavenumber difference between the antisymmetric (ν_{as} and $\nu_{as'}$) and symmetric stretching vibrations (ν_s and $\nu_{s'}$) of the carboxylate groups in different ion-cross-linked binders. (f) The viscosity test of binder aqueous solutions with different metal ions added. (g) Schematic illustration of the coordination mode of metal ions with side-chain carboxylate groups in a conductive binder.

surrounding various metal ions can be categorized into short-range (1−8 Å) and long-range regimes. In the short-range, a higher CN often indicates stronger intramolecular interactions between metal ions and carboxylate groups on the same polyfluorene chain, which is unfavorable for effective cross-linking. Within this range, Mg^{2+}, mainly exhibiting monodentate coordination, shows a higher CN, whereas Fe^{3+}, associated with multidentate bridging coordination, presents the lowest. In contrast, the long-range CN reflects interchain coordination, which is critical for reinforcing the polymer network. Fe^{3+} and Zr^{4+} have the highest long-range CNs, indicating stronger interchain interactions, while Ca^{2+} and Mg^{2+} contribute less significantly. These results highlight that multidentate bridging coordination plays a more important role in enhancing interchain connectivity than monodentate coordination.

To validate the simulation results, experimental analyses were conducted on cross-linked systems based on the aforementioned metal ions. The Fourier transform infrared spectroscopy (FTIR) spectra (Figure 2d) show that upon the introduction of metal ions, the characteristic peaks of carboxylic acid dimers at 1670 cm^{-1} diminished, while new peaks (a_1/a_2, and s_1/s_2) emerged, corresponding to the asymmetric stretching vibration (ν_{as}) and symmetric stretching vibration (ν_s) of the carbonyl group in the COO^-, respectively.[18,19] The distinct positions of these peaks are associated with different coordination modes of the carboxylate group. Specifically, when the wavenumber difference between the asymmetric and symmetric stretching vibrations of COO^-

https://doi.org/10.1021/jacs.5c22740
J. Am. Chem. Soc. 2026, 148, 7919−7930

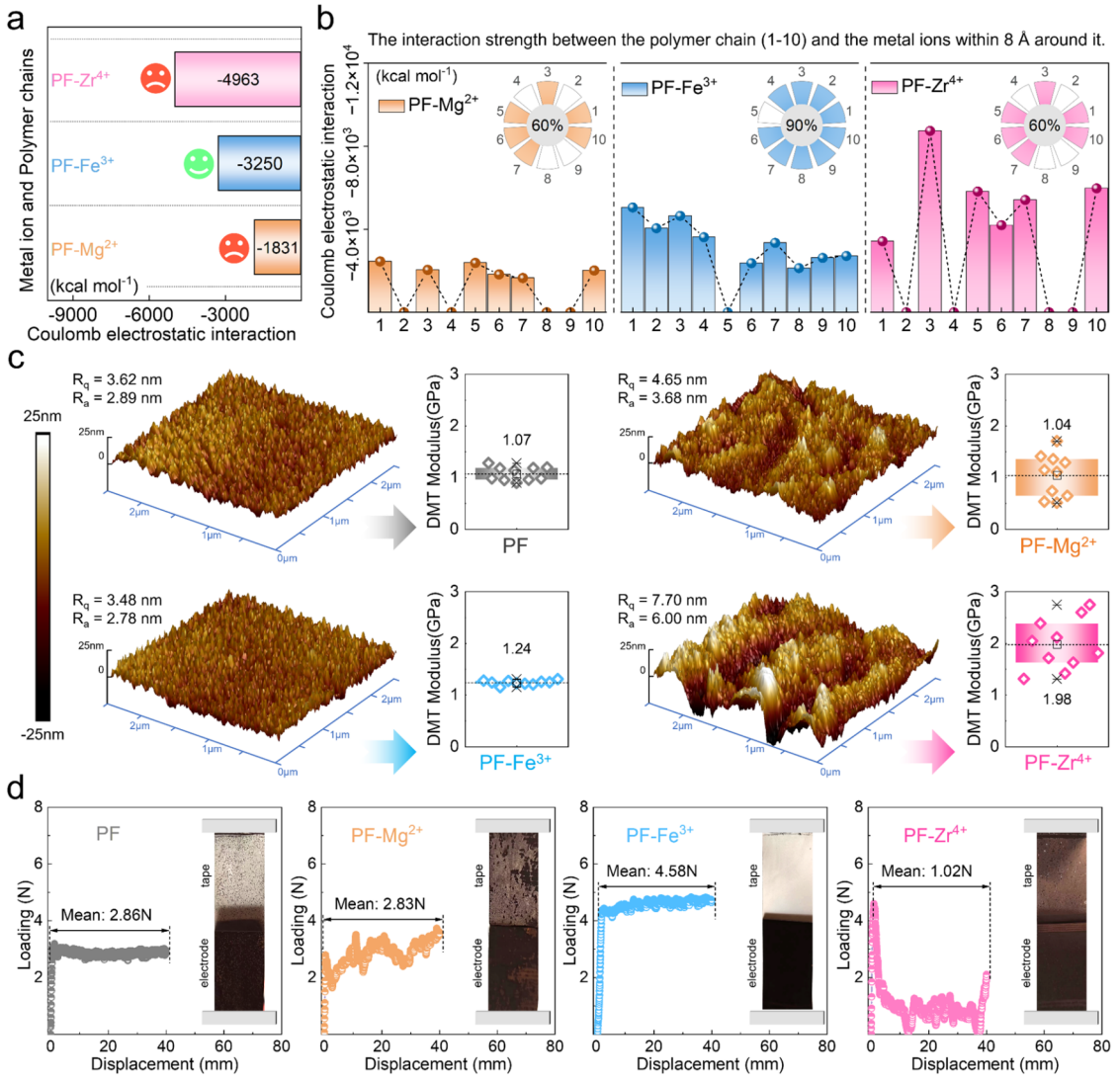

Figure 3. Mechanical strength and uniformity of the binder network with different cross-linking metal ions. (a) The Average value of the coulomb electrostatic interaction strength between metal ions and binder chains was obtained through MD simulation. (b) In the MD simulation results, the coulomb electrostatic interaction strength between the polymer chain (1−10) and the surrounding metal ions within an 8-Å range. (c) DMT modulus and roughness of the ion-cross-linked binder membranes. (d) The 180° peeling profiles of the Si electrodes.

($\nu_{as}-\nu_{s}$) falls within the range of 100−150 cm^{-1}, a multidentate bridge coordination mode is suggested; when the wavenumber difference reaches 200 cm^{-1}, monodentate coordination becomes dominant.[18] Based on this criterion, the stretching band separation results (Figure 2e) show that carboxylate groups coordinated with Mg^{2+} and Ca^{2+} exhibit monodentate coordination, while Fe^{3+} forms exclusively multidentate coordination. For In^{3+} and Zr^{4+}, both coordination modes coexist.

Additionally, viscosity tests (Figure 2f) of aqueous binder solutions at equal concentrations show a decrease in viscosity upon addition of Mg^{2+} and Ca^{2+}. This is attributed to their tendency to form intramolecular interactions with the carboxylate groups on the same molecular chain, predominantly through monodentate coordination. In contrast, the addition of other metal ions leads to increased solution viscosity, indicating enhanced intermolecular interactions. However, excessively strong cross-linking can hinder stress dissipation in electrodes, as will be discussed below. The viscosity (Figure S3) of the prepared Si slurry likewise exhibits the same trend, and the appropriate slurry viscosity is conducive to the formation of uniform electrodes. Therefore, the above experimental findings are consistent with the coordination behaviors predicted by the MD simulations (Figure 2g): appropriate multidentate bridging coordination is essential to strengthen intermolecular interactions without compromising mechanical adaptability. Among the tested ions, Fe^{3+} emerges as the most effective in achieving this balance.

2.2. Construct the Robust and Homogeneous Binder Network

To evaluate the influence of metal ions on the mechanical properties and uniformity of ion-cross-linked binders, MD simulations were employed to analyze the Coulombic electrostatic interaction between metal ions and polymer chains (Figure S4). The average interaction strength between the introduced ions and each polyfluorene chain (without imposing a distance constraint) was quantified (Figures 3a and S5). Due to predominant intramolecular interactions, Mg^{2+} and Ca^{2+} exhibit weak interactions with polymer chains, resulting in inefficient cross-linking. In contrast, Zr^{4+} forms

https://doi.org/10.1021/jacs.5c22740
J. Am. Chem. Soc. 2026, 148, 7919−7930

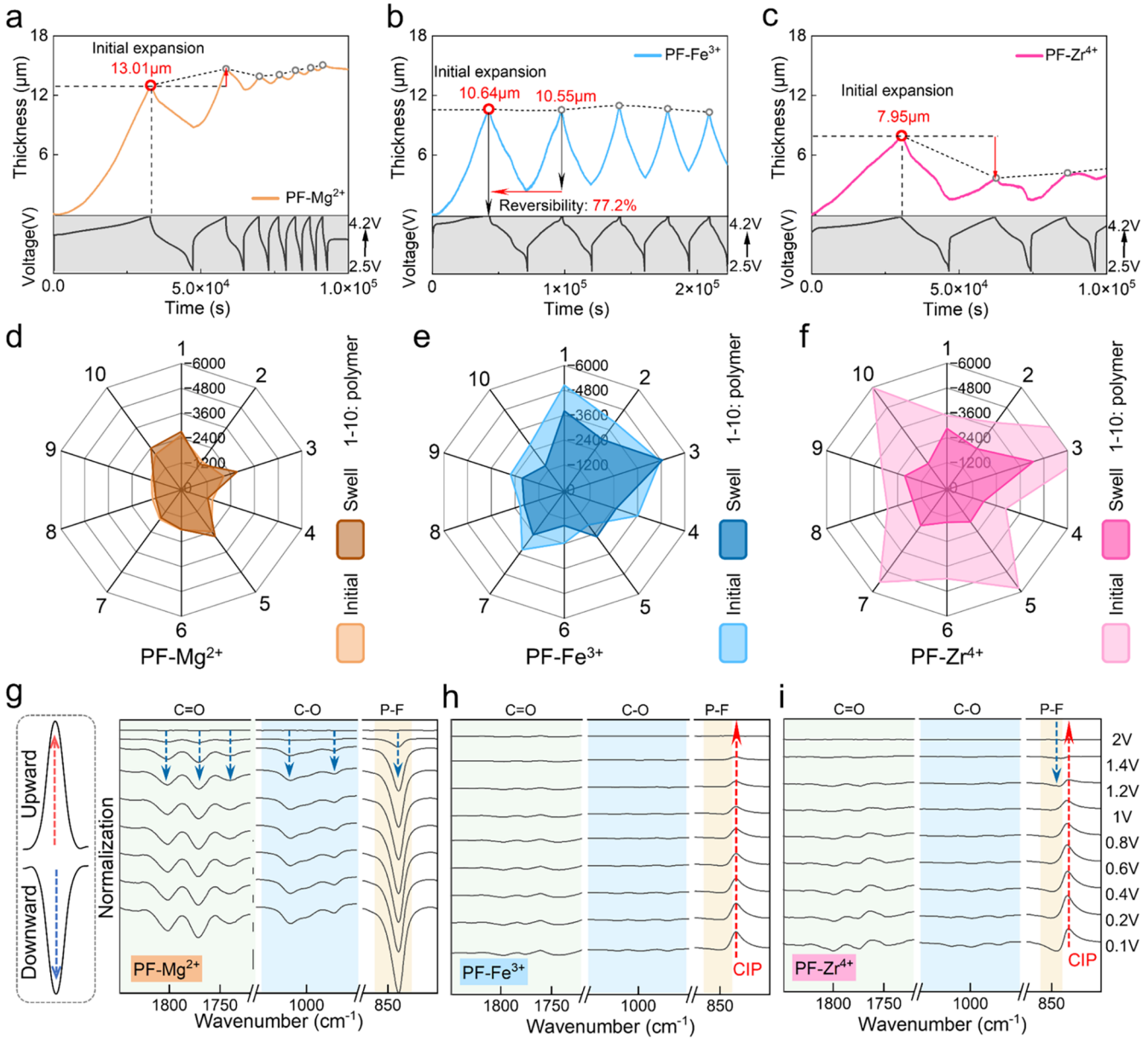

Figure 4. Compare the structure stability of the Si electrodes using various ion-cross-linked binders. Expansion rate curves of Si electrodes with different ions added (a) Mg^{2+}, (b) Fe^{3+}, (c) Zr^{4+}. By simulating the expansion process of the binder systems, the variation of coulomb electrostatic interaction strength (unit: kcal mol^{-1}) between metal ions and polymer chains in different ion-cross-linked binder systems ((d) Mg^{2+}, (e) Fe^{3+}, (f) Zr^{4+}) was explored using MD simulation. In-situ FTIR spectra of (g) Mg^{2+}, (h) Fe^{3+}, and (i) Zr^{4+} electrodes during the initial galvanostatic discharge process (from 2 to 0.1 V). The downward peak signifies a decrease in concentration, whereas the upward peak indicates an increase.

excessively strong intermolecular interactions, leading to overcross-linking and increased rigidity. Notably, Fe^{3+} and In^{3+} exhibit intermediate interaction strengths, which are consistent with the coordination strengths expected from the coordination configurations illustrated above. Thus, trivalent cations exhibit moderate ion-binding strength through maximizing intermolecular interactions. To better understand how ions interact with the polymer, we examined each polymer chain in the simulation box based on the equilibrated configurations obtained from MD simulation results. Specifically, we checked whether there were metal ions within 8 Å (determined from the RDF analysis between polymer chains and cations, Figure S6) of each chain and calculated the strength of their interactions (Figures 3b and S7). Approximately 90% of the polymer chains have Fe^{3+} nearby, indicating that Fe^{3+} is uniformly dispersed throughout the system and plays its cross-linking role effectively. In contrast, Mg^{2+} tends to cluster around only a few chains, limiting its ability to link different chains together. Similarly, Zr^{4+} also gathers near specific chains, resulting in strong local interactions. Differing from Mg^{2+}, the interactions between Zr^{4+} and polymer chains are so strong that they cause excessive local cross-linking, which disrupts the uniformity of the binding network.

Atomic force microscopy (AFM) was employed to characterize the morphology and mechanical properties of typical polymer films containing Mg^{2+}, Fe^{3+}, or Zr^{4+} (Figure 3c). The addition of Mg^{2+} leads to an increase in surface roughness, with R_q (root-mean-square roughness) and R_a (arithmetic mean roughness) reaching 4.65 and 3.68 nm, respectively, likely stemming from intramolecular interactions,

https://doi.org/10.1021/jacs.5c22740
J. Am. Chem. Soc. 2026, 148, 7919−7930

which are unfavorable for electrode fabrication. The corresponding Derjaguin-Muller-Toporov (DMT) measurements further showed large variations in modulus with no significant improvement in average mechanical strength. The polymer film incorporating Zr^{4+} exhibits even higher roughness (R_q = 7.70 nm, R_a = 6.00 nm), reflecting more pronounced surface undulations. While the overall modulus increased due to strong intermolecular interactions, localized stiffness variations persisted, likely due to excessive intramolecular cross-linking. By contrast, the Fe^{3+}-containing polymer formed a smoother film with uniform mechanical properties, attributed to balanced multidentate coordination and a more homogeneous interaction network, resulting in both improved mechanical strength and favorable film-forming characteristics.

Next, to assess dispersion behavior in slurries, ζ-potentials of Si slurries prepared with ion-cross-linked binders were measured (Figures S8−S9). The slurry with Fe^{3+}-cross-linked binder exhibited a significantly higher absolute ζ-potential than those with Mg^{2+} or Zr^{4+}, indicating superior particle dispersion. Additionally, the narrower intensity distribution peak in the Fe^{3+}-containing slurry suggests a more uniform surface potential, which helps suppress particle agglomeration, thereby promoting the uniform adhesion of anode particles to the current collector. To verify this improved adhesion, electrode peeling tests were carried out (Figure 3d). The peeling force of the Si electrode with Mg^{2+}-cross-linked binder was similar to the pristine electrode, but exhibited more uneven Si particle detachment. In contrast, Fe^{3+}-cross-linked binders significantly improved mechanical strength, resulting in a higher peeling force (4.58 N). Although Zr^{4+} increased the polymer modulus, it led to reduced peel resistance owing to the increased rigidity of the polymer film. Furthermore, extensive coordination between Zr^{4+} and carboxylate groups weakened polymer−particle and polymer-collector adhesion, leading to a more pronounced detachment of Si particles from the copper foil. Moreover, cohesive and interfacial adhesion strengths constitute critical parameters for evaluating binder performance,[20,21] which were further investigated by micrometer-scale scratch tests. As shown in Figure S10, the Fe^{3+}-cross-linked binder exhibits a higher friction coefficient, indicative of its superior adhesive capability. These results highlight that for carboxyl-rich polymers, selecting ions that can form multidentate coordination with $-COO^-$ can facilitate the formation of a robust and homogeneous cross-linked network in the electrodes.

2.3. Reinforce Structural Stability and Reversibility of Si Electrodes

Based on the above analyses, we further investigated how different binders affect the actual electrochemical processes. In-situ expansion tests using a coin-type mold (Figures 4a−c and S11−S12) were conducted to evaluate how different coordination structures influence the ability of Si anodes to accommodate volume changes. In the thickness variation profile, the ascending segment corresponds to the electrode expansion during lithiation, whereas the descending segment corresponds to the electrode contraction during delithiation. The reversibility of the amplitude of this curve reflects the reversibility of the electrode structure.[22−24] The Mg^{2+}-cross-linked electrode exhibits a thickness increase of 13.01 μm after the initial lithiation, further expanding to 14.68 μm in the second cycle, indicating poor structural integrity of the electrode and a potentially detrimental effect. In comparison, the Fe^{3+}-cross-linked electrode shows a smaller initial expansion of 10.64 μm than the pristine electrode (12.70 μm), suggesting effective suppression of swelling by the binding network. Despite partial polymer network reconstruction during the first cycle, structural stability was maintained, contributing to higher reversible capacity and dimensional reversibility (77.2%) during the second lithiation. The Zr^{4+}-cross-linked electrode exhibited the initial expansion (7.95 μm), reflecting high stiffness. However, capacity decreased during the second lithiation, likely due to polymer network breakdown caused by structural inhomogeneity, which led to the detachment of Si particles from the conductive matrix.

Then, MD simulations were employed to evaluate the ability of various cross-linked binders to withstand the volumetric expansion of Si. After a period of 10 ns, the ion-polymer interactions within the simulation box were analyzed (Figure 4d−f), where negative pressure was applied to the simulated box to mimic tensile stress, forcing molecular chains to separate. In the Mg^{2+}-cross-linked system, electrostatic interactions remain nearly unchanged due to dominant intrachain coordination, reflecting poor resistance to expansion. The Zr^{4+}-cross-linked binder initially exhibited strong ion-polymer interactions, but these weakened significantly under stress, indicating limited resilience against volume expansion. By comparison, the Fe^{3+}-cross-linked binder system maintained moderate and stable interactions throughout the process. Notably, it also exhibited the highest average Coulombic interaction strength (Figure S13), suggesting that multidentate coordination with Fe^{3+} forms a robust and adaptable elastic cross-linked network capable of accommodating volume fluctuations and supporting a stable, reversible electrode structure.

The repeated and intense expansion of Si anodes not only causes structural collapse but also triggers continuous side reactions between the electrolyte and the newly exposed Si surfaces. To investigate how suppressing irreversible volume expansion affects the stability of the SEI, which is formed as a product of electrolyte reduction,[25,26] we studied electrolyte decomposition on the surfaces of anodes with different binders using in situ FTIR. Spectra at open-circuit voltage were used as the background; downward peaks indicate electrolyte consumption, whereas upward peaks correspond to the formation of new species.[27,28] With the decrease in voltage, the attenuation of signals corresponding to C═O (1700−1850 cm^{-1}), C−O (950−1040 cm^{-1}) and the P−F (840 cm^{-1}) indicates pronounced decomposition of solvents and $LiPF_6$ (Figure S14).[29,30] Specifically, the characteristic absorption bands at 1801 cm^{-1}, 1771 cm^{-1}, and 1741 cm^{-1} (Figure S15) are, respectively, attributable to the carbonyl moieties of fluoroethylene carbonate (FEC), ethylene carbonate (EC), and diethyl carbonate (DEC). Combining the in situ electrode expansion results, it can be concluded that the insufficient mechanical constraint in the Mg^{2+}-cross-linked electrode leads to continuous SEI growth, as evidenced by the pronounced electrolyte decomposition peaks (Figure 4g). Whereas the Fe^{3+}-cross-linked binder effectively encapsulates Si particles, mitigating the side reactions. Consequently, only minor carbonate decomposition was observed with minimal consumption of $LiPF_6$ (Figure 4h). The emerged positive peak at 834 cm^{-1} indicates formation of contact ion pairs (CIPs, i.e., one PF_6^- directly coordinating to a single Li^+ cation),[31−33] and such an anion-rich interfacial environment is likely to promote the formation of a stable SEI for Si-based anodes.[31,34,35] The

https://doi.org/10.1021/jacs.5c22740
J. Am. Chem. Soc. 2026, 148, 7919−7930

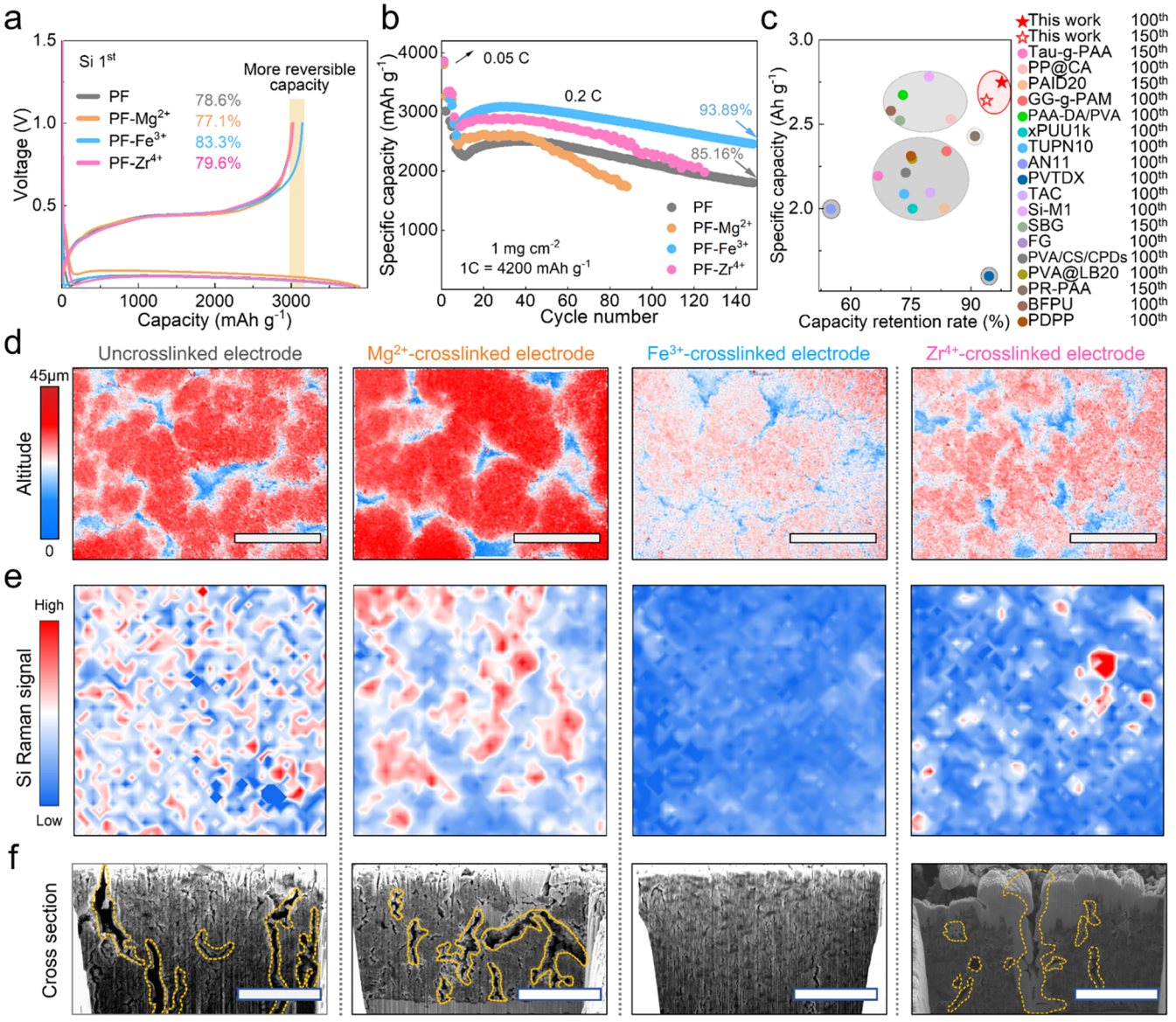

Figure 5. Long-cycle electrochemical performance and structural stability of Si electrodes using various binders. (a) Initial galvanostatic discharge/charge profiles (0.05C). (b) Cycling performance of the electrodes at the rate of 0.2 C. (c) Electrochemical performance comparison between our work and previously reported typical binders for Si electrodes. (d) Altitude difference mapping images obtained by 3D confocal microscopy. (scale bar = 100 μm). (e) Raman mappings of cycled electrodes (Test area: 40 μm × 40 μm square) created by plotting the sum of the area of the Si Raman band as a function of position range from 380 to 540 cm^{-1}. (f) The FIB-SEM test is used to obtain the cross-sectional view SEM images of the Mg^{2+}, Fe^{3+}, Zr^{4+}, and pristine electrodes (scale bar = 10 μm).

Zr^{4+}-cross-linked binder also reduced decomposition compared to Mg^{2+} and pristine systems (Figure 4i), but was less effective than Fe^{3+}, likely due to the inferior structural reversibility of the electrode. In short, the stable and reversible electrode framework constructed by the Fe^{3+}-cross-linked binder forms a stable and elastic network that not only adapts to large volume fluctuations but also limits interfacial side reactions that are difficult to control on the particle surface, stabilizing the interphasial structures of Si electrodes.

2.4. Improve Electrochemical Performance of Si Electrodes

The electrochemical performance of Si electrodes fabricated using conductive binders cross-linked by different ions was systematically evaluated. The initial voltage-capacity curves (Figure 5a) reveal that the Fe^{3+}-cross-linked electrode exhibits a higher first-cycle discharge specific capacity (3145 mAh g^{-1}) and the highest initial Coulombic efficiency (ICE) of 83.3%, which may be attributed to the cross-linked binder network's superior ability to accommodate Si expansion, thereby maintaining a robust conductive network that mitigates particle detachment and deactivation. The long-cycle performance (Figures 5b and S16) shows that the Fe^{3+}-cross-linked electrode retains a remarkable discharge specific capacity of 2642 mAh g^{-1} after 150 cycles, corresponding to a high capacity retention of 93.9% relative to the sixth cycle (2814 mAh g^{-1}), which significantly surpasses that of the pristine electrode (2057 mAh g^{-1}, 85.2%). Notably, the amount of metal ions introduced directly dictates the cross-linking degree of the binder, and both excessive and insufficient additions impede the full realization of the electrode capacity. Consequently, the ratio of 60:1 (Figure S17) was preliminarily identified as an appropriate choice.

https://doi.org/10.1021/jacs.5c22740
J. Am. Chem. Soc. 2026, 148, 7919−7930

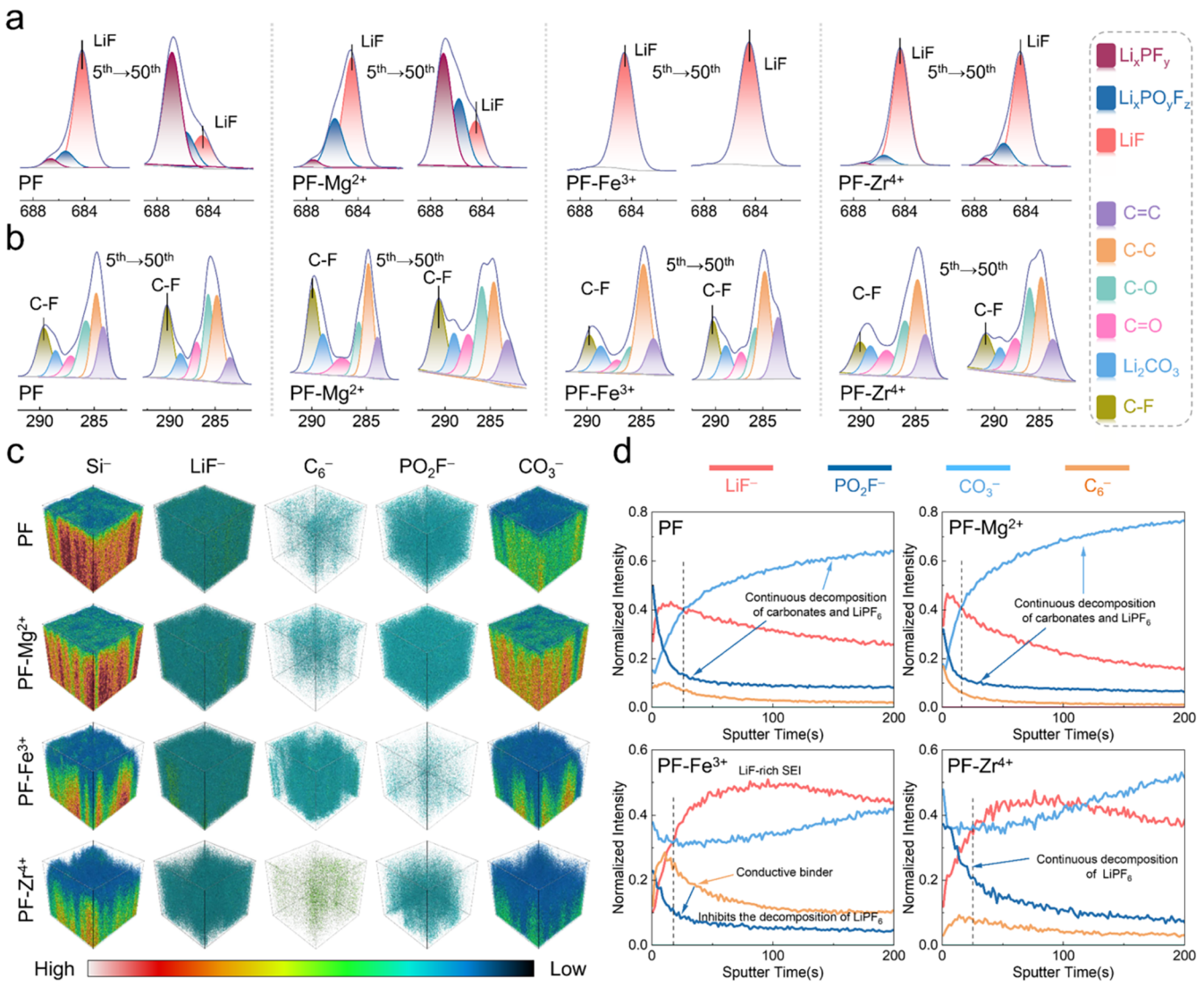

Figure 6. Composition of the SEI layer on the surface of different silicon electrodes. High-resolution XPS F 1s (a) and C 1s (b) spectra of different electrodes after 5 and 50 cycles. (c) TOF-SIMS three-dimensional distributions of the cycled Si electrodes using different ion-cross-linked binders. (d) The depth profiles of various secondary ion fragments.

The Coulombic efficiency curves (Figure S18) further demonstrate that, after five activation cycles, the Fe^{3+}-cross-linked electrode achieved a high Coulombic efficiency of 99.1% and maintains this stability throughout subsequent cycles, outperforming the pronounced fluctuations observed for the other electrodes. Given that minor fluctuations in Coulombic efficiency are commonly associated with SEI instability, the resilient binding network is proposed to suppress irreversible electrode expansion, thereby inhibiting continuous SEI growth. The differential capacity (dQ/dV) curves (Figure S19) after 50 cycles further reveal that, compared with the pristine electrode, the Fe^{3+}-cross-linked electrode exhibits lower overpotentials, indicating accelerated lithiation/delithiation kinetics and resulting in enhanced rate performance (Figure S20). In contrast, the delithiation peaks of other electrodes shift positively, while the lithiation peaks shift negatively, suggesting hindered Li^+ insertion and extraction owing to inferior structural and interfacial stability. To investigate the performance of Fe^{3+}-cross-linked binder in high-loading electrodes, we carried out a series of additional experiments. By increasing the areal loading of Si to as high as 1.53 mg cm^{-2} (Figure S21), the cycling stability remains outstanding after 100 cycles (2400 mAh g^{-1}, 93.8%). Furthermore, high-rate cycling tests demonstrate that the Fe^{3+}-cross-linked electrode also delivers higher discharge capacity (2571 mAh g^{-1}) after 100 cycles (Figure S22). When the electrochemical performance of the silicon electrodes was further evaluated using LCO||Si coin-type full cells, the Fe^{3+}-cross-linked cell, as anticipated, retained 96% of its capacity over 150 cycles (Figure S23). Compared with recently reported advanced binders (Figure 5c,and Table S1),[36−53] the Fe^{3+}-cross-linked binder forms a stable electrode architecture via multidentate bridge coordination with carboxylate groups, delivering superior capacity retention (97.7% after 100 cycles) and sustained high specific capacity. Furthermore, when applied to SiO_x electrodes (Figure S24), this binder maintains robust structural integrity, enabling a higher discharge capacity along with excellent cycling stability and rate capability.

To establish the structure-performance relationship, 3D confocal microscopy was jointly employed to observe electrode morphology (Figures 5d and S25). The surface morphology of the electrodes appears similar prior to cycling; however, slight

https://doi.org/10.1021/jacs.5c22740
J. Am. Chem. Soc. 2026, 148, 7919−7930

agglomeration can be observed on the Mg^{2+}/Zr^{4+}-cross-linked electrodes, consistent with the previously discussed slurry dispersion quality. After 50 cycles, both Mg^{2+}/Zr^{4+}-cross-linked electrodes exhibit pronounced cracking and surface heterogeneity, suggesting disrupted electrode structure. Raman mapping of cycled electrodes (Figures 5e and S26) further shows that the unstable structures of the un-cross-linked and Mg^{2+}-cross-linked binders lead to significant silicon exposure, whereas the Fe^{3+}-cross-linked binder effectively protects the electrode surface, minimizing silicon particle exposure to the electrolyte.[54] Next, focused-ion beam scanning electron microscopy (FIB-SEM) was employed to investigate the internal structure of the electrode (Figure 5f). Both the un-cross-linked and Mg^{2+}-cross-linked electrodes exhibit numerous continuous internal grooves, which are attributed to the inability of Mg^{2+} to enhance the mechanical strength of the binder. On the contrary, intramolecular interactions introduced internal stress, accelerating fracture propagation and exacerbating volume expansion. The Zr^{4+}-cross-linked electrode also shows severe internal fractures extending outward. Such structural damage triggers parasitic side reactions and promotes excessive SEI growth, which impedes Li^+ transport and degrades battery performance. In comparison, the multidentate bridge coordination formed by Fe^{3+} and COO^- constructs a uniform and robust cross-linked network that effectively dissipates stress and adapts to the expansion of Si particles. This results in a structurally stable and reversible electrode, with minimal internal cracking and maintained electronic connectivity, thereby preventing electrode failure.

2.5. Stabilized Interphases on Si Electrodes

As a critical factor affecting the performance of silicon anodes, the evolution of the SEI is also influenced by structural reversibility. X-ray photoelectron spectroscopy (XPS) was employed to track the SEI evolution from 5 to 50 cycles. After 5 cycles, XPS F 1s spectrum (Figure 6a) reveals LiF as the dominant SEI component on pristine electrodes, with minor $LiPF_6$ decomposition products ($Li_xPF_y/Li_xPO_yF_z$). The Mg^{2+}-cross-linked electrode shows more decomposition products derived from $LiPF_6$ and fluoroethylene carbonate (indicated by the C−F signal peak, Figure 6b), consistent with in situ FTIR results. In contrast, the Fe^{3+}-cross-linked electrode exhibits the highest LiF content in the SEI. Due to LiF's high stiffness and weak silicon adhesion, this SEI reinforces the electrode network, mitigating silicon volume changes while enhancing ion transport and passivating the surface.[25,26,55] After 50 cycles, the un-cross-linked and Mg^{2+}-cross-linked electrodes accumulated more $LiPF_6$ decomposition products, suggesting uncontrolled interfacial side reactions. The Zr^{4+}-cross-linked electrode retained higher LiF levels but included some $Li_xPO_yF_z$ and C−O containing organics. In contrast, the Fe^{3+} system maintained a stable, LiF-rich SEI, suppressing electrolyte decomposition and boosting silicon electrode performance.

Furthermore, time-of-flight secondary ion mass spectrometry (TOF-SIMS) was used to explore the spatial distribution of the chemical components within the SEI. 3D reconstruction patterns (Figure 6c) reveal strong Si^- signals on the surfaces of un-cross-linked and Mg^{2+}-cross-linked electrodes, indicating exposed Si particles, consistent with Raman mapping. In contrast, Zr^{4+}/Fe^{3+}-cross-linked binders effectively preserve electrode integrity. Intense PO_2F^- and CO_3^- signals indicate pronounced lithium salt and carbonate decomposition in un-cross-linked and Mg^{2+}-cross-linked systems—consistent with XPS data.[27,56] Additionally, the C_6^- fragment pattern associated with polyfluorene confirms that the Fe^{3+}-cross-linked binder maintains complete particle coverage after cycling, preserving the electrode integrity. The optimal SEI architecture positions LiF in the inner region, where it accommodates particle expansion while supporting continuous SEI growth.[28,57] Depth profiling of secondary ion fragments (Figure 6d) validates this favorable structure in Fe^{3+}/Zr^{4+}-cross-linked electrodes. The stronger binder signal detected at the surface further underscores the dual function of the Fe^{3+} multidentate coordination network: reinforcing the electrode framework and promoting the formation of a favorable outer SEI. The remaining binder signal detected at the surface further highlights the dual role of the Fe^{3+}, thereby suppressing $LiPF_6$ decomposition. By contrast, the pronounced accumulation of LiF and PO_2F^- species in the outer SEI of the other electrodes reflects persistent electrolyte decomposition at the Si surface. Temperature-dependent EIS (Figure S27) and Arrhenius analysis (Figure S28) show that the SEI of the Fe^{3+}-cross-linked electrode maintains a low Li^+ diffusion barrier, confirming suppression of excessive SEI growth. The Fe^{3+}-cross-linked binder network thus provides both structural reversibility and interfacial stability to silicon electrodes, ensuring continuous electron transport and rapid Li^+ diffusion.

3. CONCLUSION

In this work, we systematically analyzed the interactions between various metal ions and carboxyl groups, revealing the key regulatory mechanisms by which ionic coordination structures dictate the polymer binder performance in silicon anodes. It is demonstrated that the multidentate Fe^{3+}-carboxylate coordination simultaneously enhances mechanical robustness while maintaining polymer dispersibility, enabling stable silicon electrodes with highly reversible volume changes. Comprehensive characterizations further reveal that this binder effectively protects silicon surfaces, suppresses electrolyte decomposition, and prevents gradual deterioration of the LiF-rich SEI during long-cycling. By stabilizing both the bulk electrode and the interfaces, the proposed binder design significantly improved the cycling stability of silicon anodes. This work establishes the structure−performance relationship of ion-cross-linked polymer networks in silicon anodes, providing theoretical guidance for designing binders adaptable to volume changes. Moreover, these interactions are governed by a multitude of intricate factors, including the effective charge density and ionic radius of the metal ions, the nature and identity of the ligands, and the often-overlooked spatial configurations. Thus, a more systematic effort to decouple and interrogate these parameters in forthcoming studies will be of substantial importance.

■ ASSOCIATED CONTENT

Data Availability Statement

The data supporting the findings of this study are included within the article and Supporting Information.

Supporting Information

The Supporting Information is available free of charge at https://pubs.acs.org/doi/10.1021/jacs.5c22740.

Detailed methods (synthesis, characterizations, electrochemical measurements, and MD simulation) and additional data include MD simulation results, micro-

https://doi.org/10.1021/jacs.5c22740
J. Am. Chem. Soc. 2026, 148, 7919−7930

scratch tests, swelling tests, FTIR spectra, Raman spectra, and electrochemical performance data (PDF)

AUTHOR INFORMATION

Corresponding Authors

Luyi Yang − *School of Advanced Materials, Peking University, Shenzhen Graduate School, Shenzhen 518055, China;* orcid.org/0000-0002-5516-9829; Email: yangly@pkusz.edu.cn

Feng Pan − *School of Advanced Materials, Peking University, Shenzhen Graduate School, Shenzhen 518055, China;* orcid.org/0000-0002-8216-1339; Email: panfeng@pkusz.edu.cn

Authors

Lu Wang − *School of Advanced Materials, Peking University, Shenzhen Graduate School, Shenzhen 518055, China*

Hao Zhang − *School of Advanced Materials, Peking University, Shenzhen Graduate School, Shenzhen 518055, China; Department of Chemistry, City University of Hong Kong, Kowloon, Hong Kong 999077, China*

Zhibo Song − *School of Advanced Materials, Peking University, Shenzhen Graduate School, Shenzhen 518055, China*

Haoliang Wang − *School of Advanced Materials, Peking University, Shenzhen Graduate School, Shenzhen 518055, China*

Yumeng Lan − *School of Advanced Materials, Peking University, Shenzhen Graduate School, Shenzhen 518055, China*

Zu-Wei Yin − *College of Energy, Xiamen University, Xiamen 361005, China;* orcid.org/0000-0002-0728-1154

Complete contact information is available at: https://pubs.acs.org/10.1021/jacs.5c22740

Author Contributions

‖L.W., H.Z., and Z.S. contributed equally to this work.

Notes

The authors declare no competing financial interest.

ACKNOWLEDGMENTS

L.Y. acknowledges financial support from the National Natural Science Foundation of China (No. 52303263). F.P. acknowledges financial support from the National Natural Science Foundation of China (No. 92472206), International Joint Research Center for Electric Vehicle Power Battery and Materials (No. 2015B01015), Guangdong Key Laboratory of Design and calculation of New Energy Materials (No. 2017B030301013), Shenzhen Key Laboratory of New Energy Resources Genome Preparation and Testing (No. ZDSYS201707281026184).

REFERENCES

(1) He, Q.; Ning, J.; Chen, H.; Jiang, Z.; Wang, J.; Chen, D.; Zhao, C.; Liu, Z.; Perepichka, I. F.; Meng, H.; Huang, W. Achievements, challenges, and perspectives in the design of polymer binders for advanced lithium-ion batteries. *Chem. Soc. Rev.* **2024**, *53* (13), 7091−7157.

(2) Dong, S.; Wang, L.; Huang, X.; Liang, J.; He, X. Functionalized Binders Boost High-Capacity Anode Materials. *Adv. Funct. Mater.* **2024**, *34* (41), No. 2404192.

(3) Yang, L.; Meng, T.; Zheng, W.; Zhong, J.; Cheng, H.; Tong, Y.; Shu, D. Advanced binder design for high-performance silicon anodes. *Energy Storage Mater.* **2024**, *72*, No. 103766.

(4) Qian, G.; Chen, X.; Lin, H.; Yang, L. Failure-detecting techniques for commercial anodes of lithium-ion batteries. *Cell Rep. Phys. Sci.* **2024**, *5* (9), No. 102153, DOI: 10.1016/j.xcrp.2024.102153.

(5) Zhu, C.; Chen, S.; Li, K.; Yin, Z.-W.; Xiao, Y.; Lin, H.; Pan, F.; Yang, L. Quantitative analysis of the structural evolution in Si anode via multi-scale image reconstruction. *Sci. Bull.* **2023**, *68* (4), 408−416.

(6) Qian, G.; Li, Y.; Chen, H.; Xie, L.; Liu, T.; Yang, N.; Song, Y.; Lin, C.; Cheng, J.; Nakashima, N.; et al. Revealing the aging process of solid electrolyte interphase on SiOx anode. *Nat. Commun.* **2023**, *14* (1), No. 6048.

(7) Yu, Y.; Yang, C.; Zhu, J.; Xue, B.; Zhang, J.; Jiang, M. An Advanced 3D Crosslinked Conductive Binder for Silicon Anodes: Leveraging Glycerol Chemistry for Superior Lithium-Ion Battery Performance. *Angew. Chem., Int. Ed.* **2025**, *64* (6), No. e202418794.

(8) Liu, Z.; Wang, Y.; Liu, G.; Yue, X.; Shi, Z.; Tan, Y.; Zhao, J.; Lei, Y.; Yan, X.; Liang, Z. Durable and Damageless Supramolecular Binder for Fast, Stable, and Sustainable Si-Based Anodes. *J. Am. Chem. Soc.* **2024**, *146* (50), 34491−34500.

(9) Wang, Z.; Yang, M.; Liu, Y.; Li, H.; Yang, D.; Liu, B.; Lu, Z.; Lin, Z. Freely-Rotatable Multidentate Molecular Anchor Enables Self-Adaptive Aqueous Binders for Lithium-Ion Batteries. *Angew. Chem., Int. Ed.* **2025**, *64* (41), No. e202515133.

(10) Li, H.; Li, X.; Zhang, K.; Liu, D.; Wang, Y.; Zhu, G.; Hu, C.; Zhang, B.; Zhou, W. A Universal Binder Enables Stable Operation of High-Capacity Electrodes for Energy-Dense Batteries. *Adv. Funct. Mater.* **2025**, *35* (n/a), No. 2505500.

(11) Yan, W.; Ma, S.; Su, Y.; Song, T.; Lu, Y.; Chen, L.; Huang, Q.; Guan, Y.; Wu, F.; Li, N. "Shooting three birds with one stone": Bi-conductive and robust binder enabling low-cost micro-silicon anodes for high-rate and long-cycling operation. *Energy Storage Mater.* **2025**, *76*, No. 104140.

(12) Wang, L.; Zhao, Y.; Zhang, H.; Wang, H.; Chen, C.; Huang, Y.; Xue, H.; Lan, Y.; Qiao, F.; Wang, J.; et al. Carbon nanotubes grafted conductive polymer constructs robust multi-scale conductive pathways for high-performance anodes. *Energy Storage Mater.* **2025**, *78*, No. 104255.

(13) He, Y.; Zhou, F.; Zhang, Y.; Lv, T.; Chu, P. K.; Huo, K. A Triple Crosslinked Binder with Hierarchical Stress Dissipation and High Ionic Conductivity for Advanced Silicon Anodes in Lithium-ion Batteries. *Small* **2024**, *20* (45), No. 2404556.

(14) Chen, S.; Song, Z.; Wang, L.; Chen, H.; Zhang, S.; Pan, F.; Yang, L. Establishing a Resilient Conductive Binding Network for Si-Based Anodes via Molecular Engineering. *Acc. Chem. Res.* **2022**, *55* (15), 2088−2102.

(15) Wang, L.; Song, Z.; Li, Y.; Huang, Y.; Zhang, H.; Yin, Z.; Xiao, J.; Zhu, C.; Zhao, Y.; Zhang, M.; et al. Establishing an elastic electron/lithium-ion transport network via in situ crosslinking for stabilizing interphases in SiOx electrodes. *Matter* **2025**, *8* (5), No. 101952.

(16) Liu, X.; Iqbal, A.; Ali, N.; Qi, R.; Qian, X. Ion-Cross-Linking-Promoted High-Performance Si/PEDOT:PSS Electrodes: The Importance of Cations' Ionic Potential and Softness Parameters. *ACS Appl. Mater. Interfaces* **2020**, *12* (17), 19431−19438.

(17) Li, C.-H.; Zuo, J.-L. Self-Healing Polymers Based on Coordination Bonds. *Adv. Mater.* **2020**, *32* (27), No. 1903762.

(18) Dean, J. A. *Lange's handbook of chemistry*; McGrawHill, Inc., 1999.

(19) Hu, M.-L.; Morsali, A.; Aboutorabi, L. Lead(II) carboxylate supramolecular compounds: Coordination modes, structures and nano-structures aspects. *Coord. Chem. Rev.* **2011**, *255* (23), 2821−2859.

(20) Son, B.; Ryou, M.-H.; Choi, J.; Lee, T.; Yu, H. K.; Kim, J. H.; Lee, Y. M. Measurement and Analysis of Adhesion Property of Lithium-Ion Battery Electrodes with SAICAS. *ACS Appl. Mater. Interfaces* **2014**, *6* (1), 526−531.

(21) Byun, S.; Yu, J.-H.; Choi, J.; Yun, S.; Roh, Y.; Dzakpasu, C. B.; Park, S. H.; Oh, J.-G.; Hong, B. K.; Lee, Y. M. Unraveling the cohesive

and interfacial adhesive strengths of electrodes for automotive fuel cells. *J. Power Sources* **2020**, *455*, No. 227928.
(22) Yoon, D.-H.; Marinaro, M.; Axmann, P.; Wohlfahrt-Mehrens, M. Study of the Binder Influence on Expansion/Contraction Behavior of Silicon Alloy Negative Electrodes for Lithium-Ion Batteries. *J. Electrochem. Soc.* **2020**, *167* (16), No. 160537.
(23) Kim, Y.; Kim, M.; Kim, N.; Cha, H.; Kim, S.; Sung, J.; Cho, J. Unraveling the impact of CNT on electrode expansion in silicon-based lithium-ion batteries. *Energy Storage Materials* **2025**, *74*, No. 103983.
(24) Vanpeene, V.; Huet, L.; Villanova, J.; Olbinado, M.; Marone, F.; Maire, E.; Roué, L.; Devic, T.; Lestriez, B. Deciphering the Benefits of Coordinated Binders in Si-Based Anodes by Combined Operando/In Situ and Ex Situ X-Ray Micro- and Nano-Tomographies. *Adv. Energy Mater.* **2025**, *15* (6), No. 2403741.
(25) Tan, J.; Matz, J.; Dong, P.; Shen, J.; Ye, M. A Growing Appreciation for the Role of LiF in the Solid Electrolyte Interphase. *Adv. Energy Mater.* **2021**, *11* (16), No. 2100046.
(26) Chen, J.; Fan, X.; Li, Q.; Yang, H.; Khoshi, M. R.; Xu, Y.; Hwang, S.; Chen, L.; Ji, X.; Yang, C.; et al. Electrolyte design for LiF-rich solid−electrolyte interfaces to enable high-performance micro-sized alloy anodes for batteries. *Nat. Energy* **2020**, *5* (5), 386−397.
(27) Wang, H.; Zhang, H.; Wang, L.; Song, Z.; Zhao, W.; Zhan, Z.; Fang, J.; Huang, Y.; Yin, Z.-W.; Pan, F.; Yang, L. Mediating Solid Electrolyte Interphase Formation Kinetics on SiOx Anodes Using Proton Acceptors. *Angew. Chem., Int. Ed.* **2025**, *64* (33), No. e202505832.
(28) Ji, Y.; Huang, Y.; Dong, Z.; Fang, J.; Liu, P.; Liu, S.; Cao, A.; Xue, H.; Chen, S.; Qiu, J.; et al. Anion Adsorption at the Inner-Helmholtz Plane Directs Cathode Electrolyte Interphase Formation. *Angew. Chem., Int. Ed.* **2025**, *64* (20), No. e202425535.
(29) Yan, Y.; Weng, S.; Fu, A.; Zhang, H.; Chen, J.; Zheng, Q.; Zhang, B.; Zhou, S.; Yan, H.; Wang, C.-W.; et al. Tailoring Electrolyte Dehydrogenation with Trace Additives: Stabilizing the LiCoO2 Cathode beyond 4.6 V. *ACS Energy Lett.* **2022**, *7* (8), 2677−2684.
(30) Huang, Y.; Ji, Y.; Zheng, G.; Cao, H.; Xue, H.; Yao, X.; Wang, L.; Chen, S.; Yin, Z.; Pan, F.; Yang, L. Tailored Interphases Construction for Enhanced Si Anode and Ni-Rich Cathode Performance in Lithium-Ion Batteries. *CCS Chem.* **2025**, *7* (2), 429−439.
(31) Luo, H.; Ji, X.; Zhang, B.; Chen, M.; Wu, X.; Zhu, Y.; Yu, X.; Wang, J.; Zhang, H.; Hong, Y.; et al. Revealing the Dynamic Evolution of Electrolyte Configuration on the Cathode-Electrolyte Interface by Visualizing (De) Solvation Processes. *Angew. Chem., Int. Ed.* **2024**, *63* (51), No. e202412214.
(32) Zou, Y.; Ma, Z.; Liu, G.; Li, Q.; Yin, D.; Shi, X.; Cao, Z.; Tian, Z.; Kim, H.; Guo, Y.; et al. Non-Flammable Electrolyte Enables High-Voltage and Wide-Temperature Lithium-Ion Batteries with Fast Charging. *Angew. Chem., Int. Ed.* **2023**, *62* (8), No. e202216189.
(33) Seo, D. M.; Borodin, O.; Han, S.-D.; Ly, Q.; Boyle, P. D.; Henderson, W. A. Electrolyte Solvation and Ionic Association. *J. Electrochem. Soc.* **2012**, *159* (5), No. A553.
(34) Yamada, Y.; Furukawa, K.; Sodeyama, K.; Kikuchi, K.; Yaegashi, M.; Tateyama, Y.; Yamada, A. Unusual Stability of Acetonitrile-Based Superconcentrated Electrolytes for Fast-Charging Lithium-Ion Batteries. *J. Am. Chem. Soc.* **2014**, *136* (13), 5039−5046.
(35) Ilic, S.; Lavan, S. N.; Connell, J. G. Anion-derived contact ion pairing as a unifying principle for electrolyte design. *Chem.* **2024**, *10* (10), 2987−3007.
(36) Shen, J.; Zhang, S.; Wang, H.; Wang, R.; Hu, Y.; Mao, Y.; Wang, R.; Zhang, H.; Du, Y.; Fan, Y.; et al. Unlocking the potential of silicon anodes in lithium-ion batteries: A claw-inspired binder with synergistic interface bonding. *eScience* **2024**, *4* (3), No. 100207.
(37) Chen, B.; Xu, D.; Chai, S.; Chang, Z.; Pan, A. Enhanced Silicon Anodes with Robust SEI Formation Enabled by Functional Conductive Binder. *Adv. Funct. Mater.* **2024**, *34* (34), No. 2401794.
(38) Kim, J.; Kim, G.; Park, Y. K.; Lim, G.; Kim, S. T.; Jung, I. H.; Kim, H. Structure-Performance Relationship of Aromatic Polymer Binder for Silicon Anode in Lithium-Ion Batteries. *Adv. Funct. Mater.* **2023**, *33* (44), No. 2303810.
(39) Li, Z.; Wu, G.; Yang, Y.; Wan, Z.; Zeng, X.; Yan, L.; Wu, S.; Ling, M.; Liang, C.; Hui, K. N.; Lin, Z. An Ion-Conductive Grafted Polymeric Binder with Practical Loading for Silicon Anode with High Interfacial Stability in Lithium-Ion Batteries. *Adv. Energy Mater.* **2022**, *12* (29), No. 2201197.
(40) Wan, X.; Kang, C.; Mu, T.; Zhu, J.; Zuo, P.; Du, C.; Yin, G. A Multilevel Buffered Binder Network for High-Performance Silicon Anodes. *ACS Energy Lett.* **2022**, *7* (10), 3572−3580.
(41) Jeong, D.; Yook, J.; Kwon, D.-S.; Shim, J.; Lee, J.-C. Interweaving Elastic and Hydrogen Bond-Forming Polymers into Highly Tough and Stress-Relaxable Binders for High-Performance Silicon Anode in Lithium-Ion Batteries. *Adv. Sci.* **2023**, *10* (31), No. 2302027.
(42) Hwang, J. H.; Kim, E.; Lim, E. Y.; Lee, W.; Kim, J.-O.; Choi, I.; Kim, Y. S.; Kim, D.-G.; Lee, J. H.; Lee, J.-C. A Multifunctional Interlocked Binder with Synergistic In Situ Covalent and Hydrogen Bonding for High-Performance Si Anode in Li-ion Batteries. *Adv. Sci.* **2023**, *10* (30), No. 2302144.
(43) Huang, W.; Wang, Y.; Lv, L.; Li, X.; Wang, Y.; Zheng, W.; Zheng, H. Prefabrication of "Trinity" Functional Binary Layers on a Silicon Surface to Develop High-Performance Lithium-Ion Batteries. *ACS Nano* **2023**, *17* (3), 2669−2678.
(44) Kwon, Y. J.; Kim, J.-O.; Vivek, E.; Kim, E.; Kim, S. H.; Kwon, T.; Lim, E.; Chae, S.; Park, M.; Eom, Y.; et al. A stress-adaptive interlinked 3D network binder for silicon anodes via tailored chemical bonds and conformation of functionalized poly(vinylidene fluoride) (PVDF) terpolymers. *Chem. Eng. J.* **2024**, *479*, No. 147860.
(45) Lin, X.; Wen, Y.; Wang, J.; Shang, H.; Liu, H.; Xu, X. Boston ivy-inspired natural-rich binder with strong adhesion for advanced silicon-based anodes. *Chem. Eng. J.* **2023**, *468*, No. 143784.
(46) Tang, J.; Wu, F.; Dai, X.; Zhou, J.; Pang, H.; Duan, X.; Xiao, B.; Li, D.; Long, J. Robust MXene adding enables the stable interface of silicon anodes for high-performance Li-ion batteries. *Chem. Eng. J.* **2023**, *452*, No. 139139.
(47) Wu, Z.; Ma, Y.; Li, S.; Que, L.; Chen, H.; Hao, F.; Tao, X.; Xing, H.; Ye, J.; Qian, D.; et al. Damage-Tolerant and Self-Repairing Web-Like Borate Type Binder Enable Stable Operation of Efficient Si-Based Anodes. *Small* **2024**, *20* (37), No. 2401345.
(48) Zhou, W.; Zhang, R.; Yu, S.; Peng, Z.; Zuo, C.; Yang, W.; Li, Y.; Wei, M. High-Branched Natural Polysaccharide Flaxseed Gum Binder for Silicon-Based Lithium-Ion Batteries with High Capacity. *Small* **2024**, *20* (36), No. 2403048.
(49) Wu, Z.; Wan, Z.; Li, Z.; Du, Q.; Wu, T.; Cao, J.; Ling, M.; Liang, C.; Tan, Y. Partially Carbonized Polymer Binder with Polymer Dots for Silicon Anodes in Lithium-Ion Batteries. *Small* **2023**, *19* (2), No. 2205065.
(50) Wang, X.; Wang, K.; Wan, Z.; Weng, Y.; Zheng, Z.; Zhao, J.; Li, H.; Qian, D.; Wu, Z.; Ling, M.; Liang, C. Inorganic/organic composite binder with self-healing property for silicon anode in lithium-ion battery. *Mater. Today Energy* **2024**, *43*, No. 101567.
(51) Choi, S.; Kwon, T.-w.; Coskun, A.; Choi, J. W. Highly elastic binders integrating polyrotaxanes for silicon microparticle anodes in lithium ion batteries. *Science* **2017**, *357* (6348), 279−283.
(52) Jiao, X.; Yin, J.; Xu, X.; Wang, J.; Liu, Y.; Xiong, S.; Zhang, Q.; Song, J. Highly Energy-Dissipative, Fast Self-Healing Binder for Stable Si Anode in Lithium-Ion Batteries. *Adv. Funct. Mater.* **2021**, *31* (3), No. 2005699.
(53) Malik, Y. T.; Shin, S.-Y.; Jang, J. I.; Kim, H. M.; Cho, S.; Do, Y. R.; Jeon, J.-W. Self-Repairable Silicon Anodes Using a Multifunctional Binder for High-Performance Lithium-Ion Batteries. *Small* **2023**, *19* (9), No. 2206141.
(54) Hu, L.; Jin, M.; Zhang, Z.; Chen, H.; Boorboor Ajdari, F.; Song, J. Interface-Adaptive Binder Enabled by Supramolecular Interactions for High-Capacity Si/C Composite Anodes in Lithium-Ion Batteries. *Adv. Funct. Mater.* **2022**, *32* (26), No. 2111560.

https://doi.org/10.1021/jacs.5c22740
J. Am. Chem. Soc. 2026, 148, 7919−7930

(55) Wang, A.; Kadam, S.; Li, H.; Shi, S.; Qi, Y. Review on modeling of the anode solid electrolyte interphase (SEI) for lithium-ion batteries. *npj Comput. Mater.* **2018**, *4* (1), No. 15.
(56) Xue, H.; Liang, Y.; Huang, Y.; Ji, Y.; Xu, Z.; Chen, X.; Wang, H.; Liu, J.; Amine, K.; Liu, T.; et al. In Situ Conversion of Artificial Proton-Rich Shell to Inorganic Maskant Toward Stable Single-Crystal Ni-Rich Cathode. *Adv. Mater.* **2025**, *37* (7), No. 2415860.
(57) Chen, S.; Deng, Z.; Li, J.; Zhao, W.; Nan, B.; Zuo, Y.; Fang, J.; Huang, Y.; Yin, Z.-W.; Pan, F.; Yang, L. Tuning Reaction Kinetics of Fluorinated Molecules to Construct Robust Solid Electrolyte Interphases on SiOx Anode. *Angew. Chem., Int. Ed.* **2025**, *64* (1), No. e202413927.

https://doi.org/10.1021/jacs.5c22740
J. Am. Chem. Soc. 2026, 148, 7919−7930